Journal of Experimental and Theoretical Physics, Vol. 97, No. 4, 2003, pp. 773–780.
Translated from Zhurnal Éksperimental'noĭ i Teoreticheskoĭ Fiziki, Vol. 124, No. 4, 2003, pp. 862–870.

SOLIDS
Electronic Properties

Temperature and Concentration Dependences of the Electronic Structure of Copper Oxides in the Generalized Tight Binding Method

A. A. Borisov*, V. A. Gavrichkov, and S. G. Ovchinnikov

Kirenskiĭ Institute of Physics, Siberian Division, Russian Academy of Sciences, Akademgorodok, Krasnoyarsk, 660036 Russia

**e-mail: alex@sme.krk.ru*

Received December 5, 2002

Abstract—The electronic structure of *p*-type doped HTSC cuprates is calculated by explicitly taking into account strong electron correlations. The smooth evolution of the electronic structure from undoped antiferromagnetic to optimally and heavily doped paramagnetic compositions is traced. For a low doping level, in-gap impurity-type states are obtained, at which the Fermi level is pinned in the low-doping region. These states are separated by a pseudogap from the valence band. The Fermi surfaces calculated for the paramagnetic phase for various concentrations of holes are in good agreement with the results of ARPES experiments and indicate a gradual change in the Fermi surface from the hole type to the electron type. © *2003 MAIK "Nauka/Interperiodica".*

1. INTRODUCTION

Knowledge of the low-energy electronic structure, i.e., the Fermi surface and the dispersion of bands both in the superconducting and in the normal state, is essential for a better understanding of the properties of high-temperature superconductors (layered cuprates). This is necessary to determine the superconductivity mechanism and to interpret the thermodynamic and transport properties. In addition, this information can be directly obtained using angular-resolution photoelectron spectroscopy (ARPES) for the compounds $Bi_2Sr_2CaCu_2O_{8+y}$ (Bi2212) [1–9], $Bi_2Sr_2CuO_{6+y}$ (Bi2201) [10, 11], and $YBa_2Cu_3O_{7-y}$ (YBCO) [12]. The most comprehensive ARPES studies have been carried out for $La_{2-x}S_xCO_4$ (LSCO) and Bi2212 in the HTSC state. Weakly doped LSCO exhibits in-gap states and the absence of a shift (pinning) of the Fermi level. As the doping level increases to above the optimal value, the Fermi surface changes from the hole type to the electron type [13]. Unfortunately, the data on weakly doped Bi2212 are scarce in view of the absence of stable materials. However, all other properties of Bi2212 (in particular, the *d* symmetry and the concentration dependence of the pseudogap and the evolution of the Fermi surface (FS) from the hole type to the electron type in the region of strong doping [13]) are similar to those observed for LSCO. Since the electron properties of high-temperature cuprates strongly depend on the doping level, it is essential to trace the evolution of the band structure of the ARPES spectra upon doping for an understanding of the main features of high-temperature superconductivity.

The conventional band theory successfully reproduces the shape of the Fermi surface in optimally doped compounds [14] such as Bi2212. However, problems exist in HTSC systems, which cannot be solved in the framework of the band theory. Indeed, in accordance with the observed phase diagram, La_2CuO_4 is an antiferromagnetic (AFM) insulator. The dielectric nature of the ground state is ensured by a strong electron–electron Coulomb interaction at a site. However, in accordance with the Wilson criterion, the band theory demonstrates that La_2CuO_4 is a paramagnetic (PM) metal, and there are no "in-gap" states of the corresponding pinning of the Fermi level in the region of weakly doped compositions. Thus, it can be concluded that the advances in the band theory in the local density functional approximation are limited to optimally and strongly doped HTSC compounds. For weakly doped and undoped compounds, it is necessary to calculate the electronic structure taking into account strong electron correlations. Earlier, we proposed a generalized tight binding method (GTBM) [15] combining the exact diagonalization of the multielectron Hamiltonian in a cell with perturbation theory for hopping between unit cells. For an undoped CuO_2 layer, the GTBM calculations correctly reproduced not only the width of the dielectric gap, but also the dispersion at the top of the valence band for $Sr_2CuO_2Cl_2$ [16].

In this study, we analyze the spectral density of states at the top of the valence band as well as the FS cross sections for doped cuprates for various hole concentrations. The results of numerical calculations and their analysis and comparison with experiments will be given below.

1063-7761/03/9704-0773$24.00

In Section 2, the GTBM will be described briefly and basic relations for dispersion and spectral density will be given. In Section 3, we describe the numerical calculations for the density of states and the dependence of the position of the chemical potential for various concentrations of the doping component both for the PM and for the AFM phase using only the parameters determined from the calculation of the dielectric state [16]. In Section 4, the cross sections of the Fermi surface and their dependence on the doping levels are considered and compared with experimental results. In Section 5, we will show that the nontrivial temperature dependence of the spectral density in cuprates can also be reproduced in computations. The results are compared with the ARPES data obtained for chlorides $Sr_2CuO_2Cl_2$ and $Ca_2CuO_2Cl_2$.

2. BRIEF DESCRIPTION OF THE GENERALIZED TIGHT BINDING METHOD

The initial Hamiltonian of the multiband *p–d* model can be written in the form [17]

$$H = H_d + H_p + H_{pd} + H_{pp}, \quad H_d = \sum_r H_d(r),$$

$$H_d(r) = \sum_{\lambda\sigma}\Bigg[(\varepsilon_\lambda - \mu)d^+_{\lambda r\sigma}d_{\lambda r\sigma} + \frac{1}{2}U_\lambda n^\alpha_{\lambda r}n^{-\sigma}_{\lambda r}$$

$$+ \sum_{\lambda'\sigma'}\Bigg(-J_d d^+_{\lambda r\sigma}d_{\lambda r\sigma'}d^+_{\lambda' r\sigma'}d_{\lambda' r\sigma} + \sum_{r'}V_{\lambda\lambda'}n^\sigma_{\lambda r}n^{\sigma'}_{\lambda' r'}\Bigg)\Bigg],$$

$$H_p = \sum_i H_p(i),$$

$$H_p(i) = \sum_{\alpha\sigma}\Bigg[(\varepsilon_\alpha - \mu)p^+_{\alpha i\sigma}p_{\alpha r\sigma} + \frac{1}{2}U_\alpha n^\sigma_{\alpha i}n^{-\sigma}_{\alpha i} \qquad (1)$$

$$+ \sum_{\alpha'\sigma'}\Bigg(-J_p p^+_{\alpha i\sigma}p_{\alpha i\sigma'}p^+_{\alpha' i\sigma'}p_{\alpha' i\sigma} + \sum_{i'}V_{\alpha\alpha'}n^\sigma_{\alpha i}n^{\sigma'}_{\alpha' i'}\Bigg)\Bigg],$$

$$H_{pd} = \sum_{\langle i,r\rangle}H_{pd}(i,r),$$

$$H_{pd}(i,r) = \sum_{\alpha\lambda\sigma\sigma'}(t_{\lambda\alpha}p^+_{\alpha i\sigma}d_{r\lambda\sigma} + V_{\alpha\lambda}n^\sigma_{\alpha i}n^{\sigma'}_{\lambda r}),$$

$$H_{pp} = \sum_{\langle i,r\rangle}\sum_{\alpha\beta\sigma}(t_{\alpha\beta}p^+_{\alpha i\sigma}\beta_{\beta j\sigma} + \text{H.c.}),$$

where $n^\sigma_{\lambda i} = d^+_{\lambda i\sigma}d_{\lambda i\sigma}$ and $n^\sigma_{\alpha i} = p^+_{\alpha i\sigma}p_{\alpha i\sigma}$. Indices r and i run through the positions of copper ($d_{x^2-y^2} \equiv d_x$, $d_{3z^2-r^2} \equiv d_z$) and oxygen (p_x, p_y, p_z) sets of localized atomic orbitals. Similarly, $\varepsilon_\lambda = \varepsilon_{d_x}$ ($\lambda = d_x$), $\varepsilon_\lambda = \varepsilon_{d_z}$ ($\lambda = d_z$) and $\varepsilon_\alpha = \varepsilon_p$ ($\alpha = p_x, p_y$), $\varepsilon_\alpha = \varepsilon_{p_z}$ ($\alpha = p_z$) are the energies of the corresponding atomic orbitals; $t_{\lambda\alpha} = t_{pd}$ ($\lambda = d_x$; $\alpha = p_x, p_y$), $t_{\lambda\alpha} = t_{pd}/\sqrt{3}$ ($\lambda = d_z$, $\alpha = p_x, p_y$) are the matrix elements of the copper–oxygen hopping; $t_{\alpha\beta} = t_{pp}$ are the matrix elements of the hopping between the nearest oxygen ions; $U_\lambda = U_d$ ($\lambda = d_x, d_z$) and $U_\alpha = U_p$ ($\alpha = p_x, p_y, p_z$) are the intraatomic Coulomb interactions at copper and oxygen; $V_{dd}(V_{pp})$ and $J_{dd}(J_{pp})$ are the energies of the intraatomic Coulomb and exchange interactions of copper (oxygen) electrons on different orbitals; and $V_{\alpha\lambda} = V_{pd}$ ($\alpha = p_x, p_y$; $\lambda = d_x, d_z$) and $V_{\alpha\lambda} = V'_{pd}$ ($\alpha = p_z$, $\lambda = d_x, d_z$) are the energies of the Coulomb repulsion between copper and oxygen. All matrix elements of the Coulomb and exchange interactions are assumed to be independent of the form of the *d*- and *p*-plane orbitals. The prime corresponds to the interaction with apical oxygen in the CuO_6 cluster.

All calculations were made using the GTBM [16] for the CuO_2 plane divided into unit CuO_6 cells. In this version, the cell symmetry coincides with the symmetry of the crystal, but there arises the problem of common oxygen belonging to two cells simultaneously.

The problem of nonorthogonality of molecular orbitals of neighboring clusters was solved explicitly by constructing the corresponding Vanier functions on the $d_{x^2-y^2}$, $d_{3z^2-r^2}$, p_x, p_y, p_z five-orbital initial basis of atomic states. In the new symmetric basis, the one-cell part of the Hamiltonian is factorized, permitting the classification of all possible one-particle excitations in the CuO_2 plane according to symmetry. The subsequent exact diagonalization of the unit cell Hamiltonian and a transition to the representation of the Hubbard operators of the unit cell make it possible to take into account the intercellular-hopping part of the Hamiltonian in perturbation theory. As a result of exact diagonalization, the cell Hamiltonian H_c for the antiferromagnetic phase assumes the form

$$H_c = \sum_{pf_G\sigma}(\varepsilon_{1pG} - \mu)X^{pp}_{f_G\sigma} + \sum_{df_G\sigma}(\varepsilon_{2qG} - 2\mu)X^{qq}_{f_G\sigma}, \qquad (2)$$

$$f_G = \begin{cases} f_A, & f \in A \\ f_B, & f \in B. \end{cases}$$

Here, p and q denote one-hole and two-hole terms of the cell and $X^{pq}_f = |p\rangle\langle q|$ are the Hubbard operators constructed on exact states of the unit cell. The energy levels of sublattices are split by the molecular field of the antiferromagnetic state: $\varepsilon_{1pA} = \varepsilon_{1p} - \sigma h$ and $\varepsilon_{1pB} = \varepsilon_{1p} - \sigma h$. The quantity $h \propto J\langle S_z\rangle$, where J is the effective

exchange interaction between nearest neighbors. With increasing doping level, the value of h decreases, vanishing in the paramagnetic phase. In this study, we confine the analysis to non-self-consistent calculation in which the magnetic (antiferromagnetic or paramagnetic) state is assumed to be preset.

The Hamiltonian of hopping between unit cells can be written in matrix form:

$$H_{cc} = \begin{pmatrix} H_{AA} & H_{AB} \\ H_{BA} & H_{BB} \end{pmatrix} = \sum_{\lambda\lambda'\sigma kmn} \gamma^*_{\lambda\sigma}(m)\gamma_{\lambda'\sigma}(n)$$

$$\times \begin{pmatrix} T^{AA}_{\lambda\lambda'}(k)X^{+m}_{k\sigma}X^{n}_{k\sigma} & T^{AB}_{\lambda\lambda'}(k)X^{+m}_{k\sigma}Y^{n}_{k\sigma} \\ T^{BA}_{\lambda\lambda'}(k)Y^{+m}_{k\sigma}X^{n}_{k\sigma} & T^{BB}_{\lambda\lambda'}(k)Y^{+m}_{k\sigma}Y^{n}_{k\sigma} \end{pmatrix} + \text{H.c.},$$

$$T^{AA}_{\lambda\lambda'}(k) = T^{BB}_{\lambda\lambda'}(k) = \frac{2}{N}\sum_{R_1} T^{AA}_{\lambda\lambda'}(\mathbf{R}_1)e^{ikR_1},$$

$$T^{AB}_{\lambda\lambda'}(k) = T^{BA}_{\lambda\lambda'}(k) = \frac{2}{N}\sum_{R_2} T^{AB}_{\lambda\lambda'}(\mathbf{R}_2)e^{ikR_2}$$

($X^m_{k\sigma}$ and $Y^n_{k\sigma}$ are the Fourier transforms of the Hubbard operators over the A and B sublattices, respectively; here, index m labels the quasiparticle band and is determined by the pair (p, q) of indices of the initial and final multielectron states $|p\rangle$ and $|q\rangle$ in Hubbard operator X^{pq} (in terms of [18], m denotes the root vector $\boldsymbol{\alpha}_m = \boldsymbol{\alpha}(p, q)$).

The corresponding dispersion relations for the band structure of quasiparticles were derived using the equations of motion for the two-time Green temperature functions constructed on the Hubbard operators,

$$G^{\lambda\lambda'}_{k\sigma} = \langle\langle c_{k\lambda\sigma} | c^+_{k\lambda'\sigma}\rangle\rangle_E = \sum_{mn}\gamma_{\lambda\sigma}(m)\gamma^+_{\lambda'\sigma}(n)D^{mn}_{k\sigma}, \quad (3)$$

where

$$\hat{D}_{k\sigma} = \begin{pmatrix} \hat{D}_{k\sigma}(AA) & \hat{D}_{k\sigma}(AB) \\ \hat{D}_{k\sigma}(BA) & \hat{D}_{k\sigma}(BB) \end{pmatrix},$$

$$D^{mn}_{k\sigma}(AB) = \langle\langle X^m_{k\sigma} | Y^n_{k\sigma}\rangle\rangle_E.$$

In the long run, in the Hubbard I approximation, the dispersion relations are defined by the equation

$$\left\| \frac{(E - \Omega^G_m)\delta_{mn}}{F^G_\sigma(m)} - 2\sum_{\lambda\lambda'}\gamma^*_{\lambda\sigma}(m)T^{PG}_{\lambda\lambda'}(\mathbf{k})\gamma_{\lambda'\sigma}(n) \right\| = 0. \quad (4)$$

This equation is an analog of the ordinary one-electron equation in the tight binding method and differs from it in the following two aspects. First, the local energy levels Ω_m are defined as resonances between multielectron states and, hence, take into account explicitly the strong correlations due to exact diagonalization of the Hamiltonian of the CuO_6 cluster. Second, the filling factors $F^G_\sigma(m) = \langle X^{pp}_{f_G\sigma}\rangle + \langle X^{qq}_{f_G\sigma}\rangle$, which are calculated self-consistently, lead to a doping dependence of both the dispersion relations and the amplitude of the quasiparticle peak in the spectral density. From the mathematical point of view, we are dealing with a generalized eigenvalue problem, in which the inverse matrix of the corresponding filling factors appears instead of the conventional "nonorthogonality matrix." Each root vector $\boldsymbol{\alpha}_m$ describes a Fermi quasiparticle with charge e and a spin of 1/2, but with a fractional spectral weight of the order of $F(m)$; their local energies are equal to $\Omega^G_m = \varepsilon_{2qG} - \varepsilon_{1pG}$.

Formula (4) is convenient for calculating the dispersion relation in the sense that it enables us to obtain all possible quasiparticle states. However, not all of these states can be observed in experiments. It is well known that the spectrum in ARPES experiments is proportional to the spectral density of quasiparticles, which can be calculated by the GTBM in the form

$$A_\sigma(\mathbf{k}, E) = -\frac{1}{\pi}\sum_\lambda \mathrm{Im}(G^{\lambda\lambda}_{k\sigma}) = -\frac{1}{\pi}\sum_{\lambda mn}\gamma_{\lambda\sigma}(m)\gamma^+_{\lambda\sigma}(n)\mathrm{Im}(D^{mn}_{k\sigma}(AA) + D^{mn}_{k\sigma}(BB)). \quad (5)$$

Owing to corresponding filling factors, the spectral density for some types of quasiparticles may be simply negligibly low or even equal to zero. Consequently, the corresponding quasiparticle peak can be missing in the experiment. The numerical calculation of spectral density by formula (5) was carried out along the principal symmetric directions of the Brillouin zone at $T = 0$. For the PM phase, the dispersion relation and the spectral density can be obtained using one-sublattice analogs of formulas (4) and (5). The band structure of the undoped CuO_2 layer in the PM phase was calculated in [19] and is shown in Fig. 1. In this case, the Fermi level lies in the forbidden band and the dielectric gap width $E_g \sim 0.2$ eV is close to the experimentally observed value. It should be noted that the dielectric ground state is due to strong electron correlations, while the gap width is mainly determined by charge transfer processes. The complex structure of the valence band is due to a large number of quasiparticles with the participation of two-

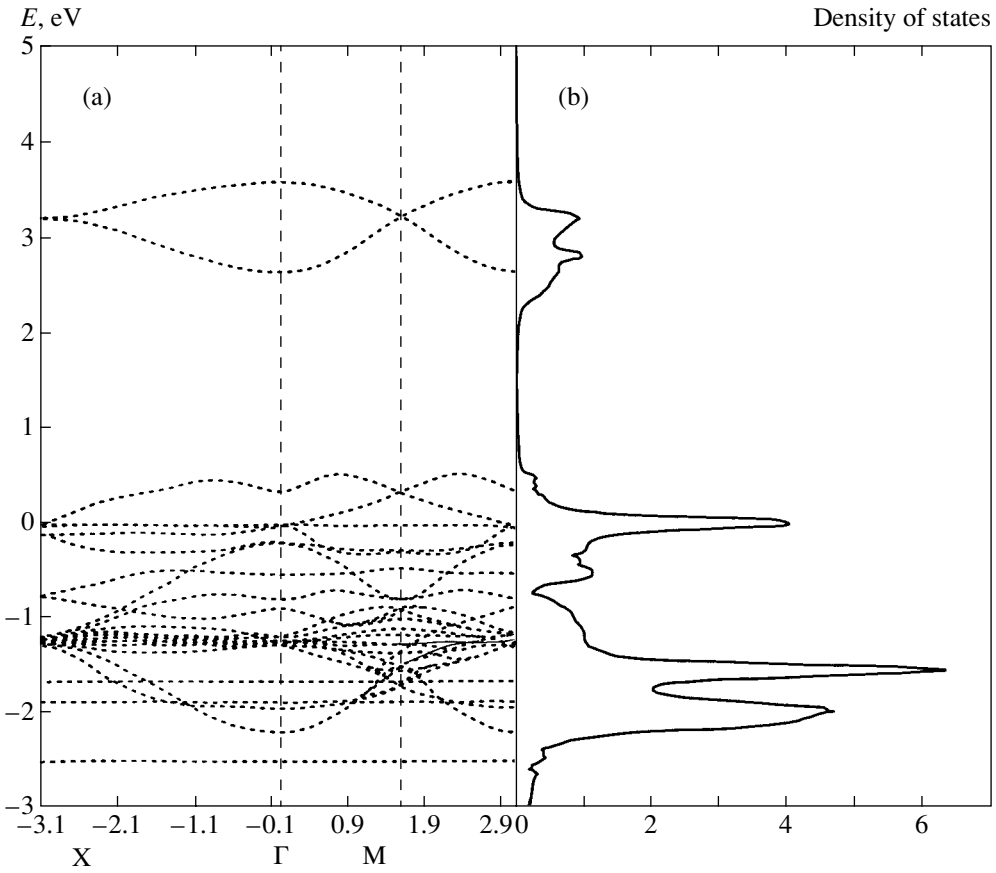

Fig. 1. Dispersion relation and the density of states of an undoped CuO_2 layer in the PM phase (borrowed from [19]).

hole states of the unit cell; the width of the valence band is approximately equal to 3 eV in conformity with the experimentally observed value for La_2CuO_4.

Following publication [19], numerous experimental studies of the band structure of cuprates were carried out using ARPES methods, which enabled us to refine the model parameters [16] and to achieve a quantitative agreement for the dispersion relation for the top of the valence band in $Sr_2CuO_2Cl_2$. We obtained the following model parameters in units of t_{pd} ($\varepsilon_{d_x} = 0$):

$$\begin{aligned} &\varepsilon_{d_z} = 2, \quad \varepsilon_p = 1.6, \quad \varepsilon_{p_z} = 0.5, \\ &t_{pp} = 0.46, \quad t'_{pp} = 0.42, \quad U_d = 9, \\ &U_p = 4, \quad U_{pd} = 1.5, \quad J_d = 1. \end{aligned} \tag{6}$$

Here, we describe the doping dependence of the electronic structure without introducing additional fitting parameters.

3. DENSITY OF STATES

Figure 2 shows the dispersion relations for the bottom of the conduction band and the top of the valence band of an undoped CuO_2 layer, calculated for the AFM phase at $T = 0$ with parameters (6). The Fermi level lies in the gap. Nondispersed levels at the bottom of the conduction band and at the top of the valence band

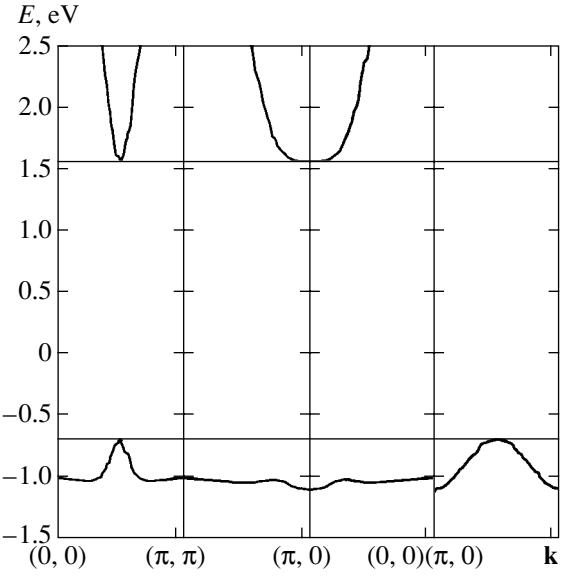

Fig. 2. Dispersion relation for the top of the valence band and the bottom of the conduction band for an undoped CuO_2 layer in the AFM phase.

show the virtual states with zero spectral weight, which were obtained in [16]. It is these levels that form, as a result of doping, the in-gap states with a spectral weight proportional to the doping level.

Figure 3 shows a part of the density of states near the top of the valence band of the CuO_2 layer doped with holes in the AFM phase. We denote by $N_1(E)$ the contribution to $N(E)$ from the top of the valence band; this contribution is characterized by a narrow peak associated with Van Hove singularities. As a result of doping, a virtual level acquires dispersion, the density $N_2(E)$ within the gap states being low in view of the smallness of the hole concentration. The in-gap states are responsible for a red shift of the top of the valence band; however, this shift is difficult to observe in experiments in view of the low spectral density. The main spectral weight $N_1(E)$ of the peak experiences a blue shift approximately equal to 0.1 eV. One more peak appearing at the "shoulder" of the main peak corresponds to a Van Hove singularity at point $\mathbf{k} = (\pi, 0)$. Naturally, only an insignificant blue shift is observed against the background of the density of states from the entire valence band (see Fig. 1) since the value of $N_1(E)$ is much smaller than the total density of states. Thus, the absorption edge at low doping levels in the AFM phase is formed with the participation of states whose presence at the top of the valence band is associated with strong electron correlations. The spectral density of such an individual state may change in the limits determined by the sum rule determined by the presence of a "constraint" (inaccessibility of a part of multielectron states due to strong electron correlations),

$$\int A_1(\mathbf{k}, E)dk = N_1(E),$$

$$\int A_2(\mathbf{k}, E)dk = N_2(E),$$

$$\int N_1(E)dE + \int N_2(E)dE = 1,$$

which were used in calculating the position of the Fermi level. Thus, the position of the Fermi level can be determined from the equation

$$x = \int_{\mu}^{\infty} N_1(E)dE + \int_{\mu}^{\infty} N_1(E)dE,$$

where the spectral density and the density of states depend on the doping component concentration. In other words, the situation takes place opposite to that in the hard band model. It can be seen from Fig. 3 that the density of states $N_2(E)$ of an impurity-type band has dips in the vicinity of $E \approx -0.8$ eV, which correspond to the pseudogap between the valence band and the virtual level. The main contribution to the formation of the

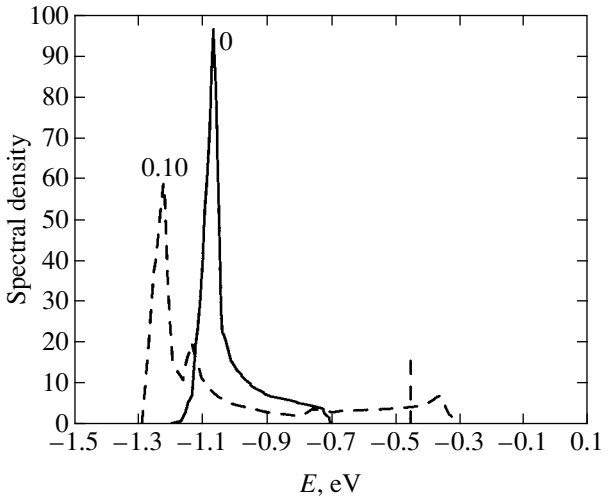

Fig. 3. Density of states of a CuO_2 layer doped with holes with concentration x in the AFM phase.

pseudogap comes from the states in the vicinity of point $(\pi, 0)$ of the Brillouin zone. For $x \sim 0.01$, for which the AFM phase is preserved after doping, the spectral weight of the in-gap state is small in view of the smallness of x. For this reason, we show in Fig. 3 for better visualization the density of states for large values of x from the range of weakly doped compositions. For $x = 0.10$, the long-range AFM order is not observed any longer, but a short-range order of the AFM type takes place in this range with a correlation length ξ_{AFM} larger than the length l of formation of the electron structure (analogous to the mean free path); l = 2–3 lattice parameters. Consequently, as a reasonable interpolation between the AFM ordering with a long-range order ($x < 0.03$) and the strongly doped paramagnetic region ($x > 0.18$), we disregard the difference between the long-range and short-range AFM order in weakly and optimally doped samples and calculate the band structure in the AFM phase; for $x > x_{opt}$, the band structure in the PM phase is calculated. The vertical dashed line in Fig. 3 shows the position of the Fermi level. The evolution of the position of the Fermi level upon doping (Fig. 4) indicates the possibility of Fermi level pinning as a result of simultaneous increase in the carrier concentration and the spectral density at a virtual level. Precisely such a behavior of the Fermi level was observed in [20] for $La_{2-x}Sr_xCuO_4$. In the PM phase, the impurity band merges with the valence band and the Fermi level for $x > 0.15$ is displaced towards the bottom of the valence band.

4. FERMI SURFACE

Figure 5 shows the dynamics of the Fermi surface cross section upon a change in the doping level for the PM phase. For lower doping levels, no agreement with the experimental data [21] could be reached. This can be explained by the necessity of a more detailed

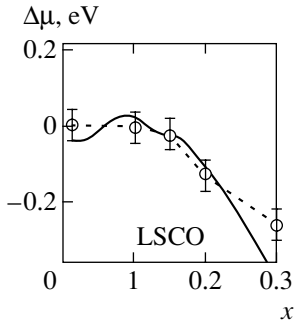

Fig. 4. Chemical potential shift as a function of the doping level. The solid curve describes the results of GTBM computations ($x < 0.15$ for the AFM phase and $x > 0.15$ for the PM phase). The experimental data for $La_{2-x}Sr_xCuO_4$ are borrowed from [20].

description of the spin system for lower doping levels. The Fermi surface is subjected more strongly to the effect of various parameters of the system and not only the chemical potential, which is an integrated characteristic. In our computations, the optimal doping level for which the Fermi level reaches a Van Hove singularity in the PM phase is observed at $x_{\text{opt}}^{T} \approx 0.55$, while the experimental value is $x_{\text{opt}}^{\text{exp}} \approx 0.18$. Assuming that we were incorrect only while determining the scale of the doping level and the evolution of the Fermi surface corresponds to the experimental results, we describe our results in units of relative doping levels $x^T = x^* x_{\text{opt}}^{T} / x_{\text{opt}}^{\text{exp}}$. Indeed, it can be seen in Fig. 5 that the results of calculations are in good qualitative agreement with experimental data. Thus, the evolution of the FS in LSCO is reproduced qualitatively in the concentration range of $x > 0.15$. Quantitative discrepancies are observed for the absolute value of x_{opt}. A departure from the Hubbard I approximation in which Eq. (4) was derived and the inclusion of short-range order spin correlations will apparently narrow the band and will lead to correct values of concentrations. An analogous conclusion was drawn for the *t–J* model in [22, 23].

5. TEMPERATURE DEPENDENCE OF ARPES SPECTRA

Kim *et al.* [24] obtained the results of a peculiar variation of ARPES spectra for $Sr_2CuO_2Cl_2$ with temperature. With increasing temperature, the height of spectral density peaks decreased and the peaks were shifted towards lower energies. For finite temperatures, the intensity of the ARPES spectra can be described as

$$I(\mathbf{k}, \omega) \propto f_F(\omega) A(\mathbf{k}, \omega),$$

where $A(\mathbf{k}, \omega)$ was calculated by formula (5) with the help of two-time Green temperature functions. Usually, the temperature dependence of the photoelectron spectra in the vicinity of the Fermi level is determined by the spread of the Fermi distribution function. However, in a system with strong correlations, additional, stronger mechanisms of temperature dependence associated with the spectral density itself come into play. In our case of the undoped CuO_2 layer, the filling factors depend on temperature in view of the temperature dependence of the population of the upper spin level $\varepsilon_{1,A}^{-\sigma}$. In the absence of spin fluctuations, we would have $\langle S_A^Z \rangle = 1/2$ and $n_1^{-\sigma} = 0$. However, zero-point spin fluctuations take place in the AFM phase even at $T = 0$, and $\langle S_A^Z \rangle = 1/2 - n_1^{-\sigma}(0)$ and $n_1^{-\sigma} = n(T)$. As the temperature increases, the occupational number $n(T)$ for the upper spin layer increases. The value of $n(T)$ can be calculated quite easily in the spin-wave approximation (which gives $n_1^{-\sigma} \approx 2$ for $T = 0$); however, experiments [24] were performed for rather high temperatures of $T \leq T_N$, at which the evaluation of the magnon concentration is a complicated problem, which is beyond the framework of this paper. For this reason, instead of $n(T)$, we calculate the spectral density at three points corresponding to

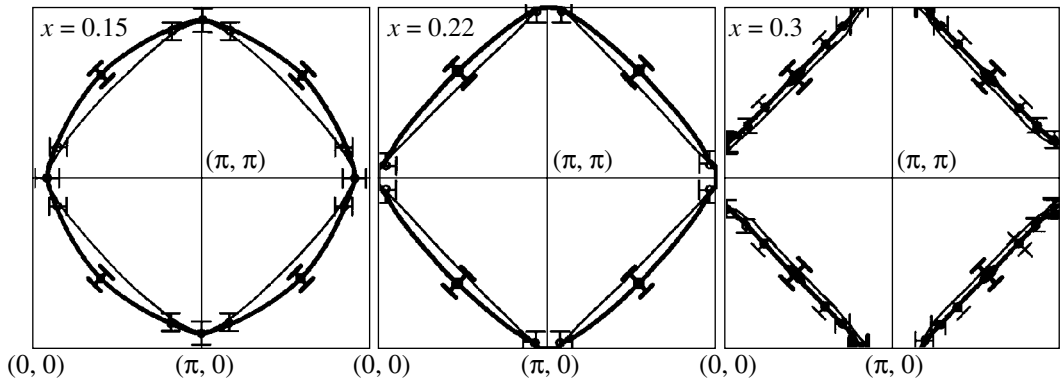

Fig. 5. Evolution of the Fermi surface upon an increase in the hole concentration in $La_{2-x}Sr_xCuO_4$. Thin curves describe the results of GTBM computations, while bold curves are ARPES spectroscopic data from [21].

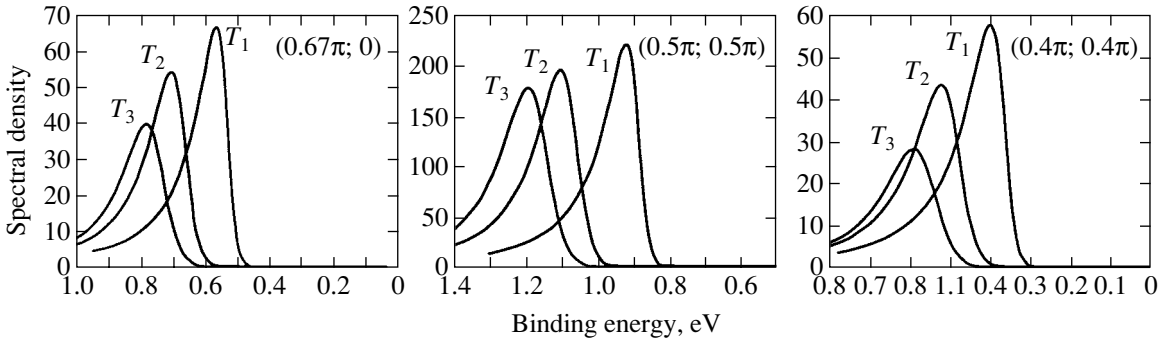

Fig. 6. Temperature dependence of the spectral density for points (2π/3; 0), (π/2; π/2), and (0.4π; 0.4π).

temperatures $T_1 < T_2 < T_3$ such that $n(T_1) = 0.3$, $n(T_2) = 0.4$, and $n(T_3) = 0.5$, point T_3 lying above T_N. It can be seen from Fig. 6 that for all three points of the Brillouin zone at which the temperature dependence of the ARPES spectra, we obtained qualitative agreement with the experiment; for $Sr_2CuO_2Cl_2$, the spectral density peak amplitude at point $\mathbf{k} = (0.67\pi; 0)$ decreases upon an increase in temperature faster than at point $\mathbf{k} = (0.5\pi; 0.5\pi)$, in accordance with the experimental data.

6. CONCLUSIONS

A systematic analysis of the evolution of the electronic structure with doping in LSCO within the GTBM reveals the following three distinct features.

First, the Fermi level in the range of low-doped *p*-type HTSC compounds is pinned by the states of a virtual level in the region of the dielectric gap and exhibits no shift. Indeed, in view of the presence of the undoped virtual CuO_2 level at the top of the valence band, which acquires a finite spectral density and dispersion as a result of doping, the Fermi level is pinned by these states and not by the valence band itself.

Second, as the dopant concentration increases in the PM phase, the evolution from the hole-type FS with the center at $k = (\pi, \pi)$ to the electron-type FS with the center at $k = (0, 0)$ takes place [21]. This scenario is reproduced in calculations. However, a discrepancy is observed between the theoretical and experimental values of x_{opt} in this case. Since the calculated values of x_{opt} for the AFM phase are lower ($x_{opt} \approx 0.28$–0.3), we believe that this discrepancy is due to the simplified description of spin correlations and hope that the correct value of x_{opt} can be obtained by taking into account the short-range spin order.

Third, in the AFM phase of HTSC compounds, our computations reproduce the pseudogap between the "impurity" band and the top of the valence band. The pseudogap is destroyed together with the impurity band upon an increase in the doping level since the dispersion of electrons in the PM phase is similar to dispersion of optimally doped HTSC compounds.

In addition, the band structure of quasiparticles and the spectral density strongly depend on the temperature in the AFM phase; the nature of this dependence is associated with the redistribution of the spectral weight between various quasiparticles upon a change in temperature. Neither the temperature nor the concentration dependence of the band structure can be obtained using the traditional one-electron band approach; these dependences are consequences of the specific band structure of quasiparticles in strongly correlated electronic systems [25].

ACKNOWLEDGMENTS

This study was supported financially by the Federal Special Program "Integration" (grant no. B0017), the Russian Foundation for Basic Research and Krasnoyarsk Regional Science Foundation "Enisei" (grant no. 02-02-97705), Russian Foundation for Basic Research (project no. 03-02-16124), INTAS (grant no. 01-0654), and the program "Quantum Macrophysics" of the Russian Academy of Sciences.

REFERENCES

1. Z.-X. Shen and D. S. Dessau, Phys. Rep. **253**, 1 (1995).
2. D. S. Marshall, D. S. Dessau, A. G. Loeser, *et al.*, Phys. Rev. Lett. **76**, 4841 (1996).
3. H. Ding, M. R. Norman, T. Yokoya, *et al.*, Phys. Rev. Lett. **78**, 2628 (1997).
4. H. Ding, M. R. Norman, J. C. Campuzano, *et al.*, Phys. Rev. B **54**, R9678 (1996).
5. H. Ding, T. Yokoya, J. C. Campuzano, *et al.*, Nature **382**, 51 (1996).
6. P. J. White, Z.-X. Shen, C. Kim, *et al.*, Phys. Rev. B **54**, R15669 (1996).
7. A. G. Loeser, Z.-X. Shen, D. S. Dessau, *et al.*, Science **273**, 325 (1996).
8. J. M. Harris, Z.-X. Shen, P. J. White, *et al.*, Phys. Rev. B **54**, 15665 (1996).
9. M. R. Norman, H. Ding, M. Randeria, *et al.*, Nature **392**, 157 (1998).
10. J. M. Harris, P. J. White, Z.-X. Shen, *et al.*, Phys. Rev. Lett. **79**, 143 (1997).

11. D. M. King, Z.-X. Shen, D. S. Dessau, *et al.*, Phys. Rev. Lett. **73**, 3298 (1994).
12. M. C. Schabel, C.-H. Park, A. Matsuura, *et al.*, Phys. Rev. B **55**, 2796 (1997).
13. A. Damascelli, D. H. Zu, and Z.-X. Shen, J. Electron Spectrosc. Relat. Phenom. **117**–**118**, 165 (2001).
14. E. G. Maksimov, Usp. Fiz. Nauk **170**, 1033 (2000) [Phys. Usp. **43**, 965 (2000)].
15. S. G. Ovchinnikov and I. S. Sandalov, Physica C (Amsterdam) **161**, 607 (1989).
16. V. A. Gavrichkov, S. G. Ovchinnikov, A. A. Borisov, and E. G. Goryachev, Zh. Éksp. Teor. Fiz. **118** (2), 422 (2000) [JETP **91**, 369 (2000)].
17. Ya. B. Gaididei and V. M. Loktev, Phys. Status Solidi B **147**, 307 (1988).
18. R. O. Zaĭtsev, Zh. Éksp. Teor. Fiz. **70**, 1100 (1976) [Sov. Phys. JETP **43**, 574 (1976)].
19. S. G. Ovchinnikov, Phys. Rev. B **49**, 9891 (1994).
20. N. Harima, J. Matsuno, A. Fujimori, *et al.*, Phys. Rev. B **64**, 220507 (2001).
21. A. Ino, C. Kim, M. Nakamura, *et al.*, Phys. Rev. B **65**, 094504 (2002).
22. N. M. Placida and V. S. Oudovenko, Phys. Rev. B **59**, 11949 (1999).
23. A. Sherman and M. Schreiber, Phys. Rev. B **65**, 134520 (2002).
24. C. Kim, F. Ronning, A. Damascelli, *et al.*, Phys. Rev. B **65**, 174516 (2002).
25. V. V. Val'kov and S. G. Ovchinnikov, *Quasi-Particles in Strongly Correlated Systems* (Sib. Otd. Ross. Akad. Nauk, Novosibirsk, 2001).

Translated by N. Wadhwa